How Does the Surface Tension Depend on the Surface Area with Coarse-Grained Models?

Florent Goujon, Alain Dequidt, Aziz Ghoufi, Patrice Malfreyt

How does the surface tension depend on the surface area with coarse-grained models ?

Florent Goujon,[†] Alain Dequidt,[†] Aziz Ghoufi,[‡] and Patrice Malfreyt[*,†]

[†]*Université Clermont Auvergne, CNRS, SIGMA Clermont, Institut de Chimie de Clermont-Ferrand (ICCF), F-63000 Clermont-Ferrand*

[‡]*Institut de Physique de Rennes, Université Rennes 1, 35042 Rennes, France*

E-mail: Patrice.Malfreyt@uca.fr

Abstract

We propose to investigate the size-effects on the surface tension calculated with coarse-grained (CG) models. We investigate different liquid-vapor (LV) and liquid-liquid (LL) interfaces with the MARTINI forcefield and orignal CG models designed for the dissipative particle dynamics (DPD) and multibody particle dynamics (MDPD) simulations. We also test a realistic CG potential developed for the DPD method to investigate the LV interface of *n*-pentane. Concerning the MARTINI forcefield, we observe a weak oscillatory effect of the interfacial tension with the surface area for the LV interfaces of *n*-octane and water. This weak dependence of the surface tension with the box dimension is also observed in the LL interface of *n*-octane-water (MARTINI, DPD) and in the LV interface of water with the MDPD model.

1 Introduction

The coarse-grained (CG) models have been widely applied in molecular simulations of biomolecules,[1] polymers[2–4] and surfactants.[5] In the CG model, the interactions are simplified with a CG particle corresponding to many atoms or molecules. These models are designed to model systems on time scales over hundred of nanoseconds that are not accessible by standard molecular simulations. Among the various CG force fields, the MARTINI force field[6–12] developed by Marrink et al. is by far the most commonly used. This model can be implemented in Monte Carlo (MC) and Molecular Dynamics (MD) simulation methods. Other CG potentials[4] are used with mesoscopic methods such as dissipative particle dynamics (DPD).[13–16]

There is an increasing need to use these CG models to calculate the interfacial tension of LV and LL interfaces. CG simulations are also important in the industry and in detergency issues because they can be applied to multi-component mixtures.[5] A key-property in the simulations of these interfacial systems is the interfacial tension. A recent review[17] shows that some CG force fields present significant deviations of the calculated interfacial tension from experiments.[18] The first simulations of the LV interface of water with the MARTINI CG model[7] produced surface tensions of 45 and 30 mN m^{-1} at 298 K obtained for small and big system sizes, respectively. For the electrostatic version of the water MARTINI model,[10] the simulated surface tension is found to be 30 mN m^{-1} while the corresponding experimental value[19,20] is 72 mN m^{-1}. The MARTINI model produces more quantitative predictions in the case of the LV interface of alkanes.[7] The surface tension of water[16] has also been calculated from the MDPD method.[15] In this work, a top-down approach has been carried out to develop of the potential parameters.

Even though the calculation of the surface tension from two-phase atomistic simulations of a slab geometry is now under control, it has been at the heart of several debates over the last 40 years.[17,21–38] Actually, these slab simulations gave rise to several debates to important methodological problems such as the range of the interatomic interactions,[31,35,39–41]

the truncation of the potential,[33,39] the mechanical and thermodynamic definitions used for the calculation of the surface tension[33,42–44] and the long-range corrections to surface tension[26–30,32–34] and to the configurational energy.[28,32,34,38,44,45] An other input parameter that may impact the value of the simulated surface tension is the size of the interfacial area. A number of works have reported the dependence of the surface tension of the Lennard-Jones (LJ) fluid on the surface area.[35,46–49] Figure 1 illustrates this dependence for the LJ fluid by showing the ratio of the surface tension γ to the surface tension γ_∞ calculated at the largest surface area.

Nowadays the CG models are extensively used to model large and complex interfacial systems where the surface tension is at the origin of the transport of matter through the interface. As a consequence, it is important to investigate the interface area dependence on surface tension to avoid spurious computational effects. To do so, we propose in a first step to study the impact of the surface area on the interfacial tension calculated by the MARTINI Model. We will investigate the LV interface of water and *n*-octane. We will complete by the LL alkane-water interface. In the CG MARTINI model, the interactions are calculated by both the truncated and shifted LJ and Coulombic potentials.[18] In the case of CG interactions treated with softer potentials, we will extent the study of the size-effects to a mesoscopic simulation method (dissipative particle dynamics, DPD) by using different shapes of CG potentials. In a first step, we plan to study the size-effects for generic DPD models for the water LV and oil-water LL interfaces. In these cases, we will use the standard conservative interactions of the DPD model and its multibody version.[15,16,50,51] In a second step, we will investigate the size-dependence of the interfacial tension of the LV interface of the *n*-pentane by using a realistic DPD potential.[52]

Since the MARTINI and the different DPD models are the most commonly used for the mesoscale modeling of complex systems, the results concerning the size-dependence of the interfacial tension of coarse-grained interfaces will be very useful for the future simulations in this field.

The paper is organized as follows. Section 2 describes briefly the different potential models, the methods of simulations and the computational details. In Section 3 we discuss the different finite-size effects of the MARTINI model for different interfaces. We complete by examining the surface area dependence of the interfacial tension for different CG DPD models. Section 4 contains our conclusions and recommendations.

2 Model and simulation methodology

2.1 MARTINI model

In the LV interface of the n-octane, the molecule[6] is described by two beads of type C_1. The bonding energy between two beads a and b is calculated by using a harmonic potential $U_{bond}(r_{ab})$

$$U_{bond}(r_{ab}) = \frac{1}{2} k_{bond}(r_{ab} - r_0)^2 \tag{1}$$

where r_{ab} is the distance between beads a and b and r_0 the equilibrium distance. The van der Waals diameter of the CG beads σ is fixed to 0.47 nm and ϵ is scaled to 75% of the original value of C_1. The values of k_{bond}, r_0, σ and ϵ are listed in Table 1.

The parameters of the polarizable version of the water MARTINI force field[10] are listed in Table 1 et can be found in Ref. 10. In the case of the modeling of the n-octane-water LL interface, the cross-interactions between water (W) and alkane (C1) beads are given in Table 1.

The molecular dynamics (MD) simulations were performed with a modified version of the DL_POLY code.[53] The changes consist of implementing the shift of the forces from $r_s = 9$ Å to $r_c = 12$ Å. The procedure is described in Ref. 18. The simulations of the LV interface were carried out in the constant-NVT statistical ensemble with the Nose-Hoover[54] algorithm using a thermostat relaxation time of 0.1 ps. For the LL interface, the simulations were performed in the constant $Np_{\mathrm{N}}AT$ statistical ensemble with the thermostat-barostat

Nose-Hoover algorithm.[55] The thermostat and barostat relaxation times were fixed to 0.1 and 5.0 ps, respectively. The normal component of the pressure tensor p_{N} was maintained to 0.1 MPa and T = 298 K. The integration timestep was fixed to 10 fs.

The different bulk liquid phases of octane and water were equilibrated separately during 2×10^7 steps of simulations (10^7 NVT steps followed by 10^7 NpT steps). For the LV simulation, L_z is elongated to form the vapor phase. For LL simulations, the bulk phases of the two liquids were joined to form the initial configuration. The equilibration phase consisted of 10^7 steps and the calculation of the average properties was carried out over 10^7 additional steps during the acquisition phase. The simulation time of the acquisition phase is then 100 ns.

2.2 DPD method

2.2.1 Generic DPD model

In the DPD method, the total force $\mathbf{f}_i$ sums three forces: a conservative $\mathbf{f}_{ij}^C$ force, a random $\mathbf{f}_{ij}^R$ force and a dissipative $\mathbf{f}_{ij}^D$ force. The conservative repulsive force $\mathbf{f}_{ij}^C$ is

$$\mathbf{f}_{ij}^C = \begin{cases} a_{ij}\, \omega_C(r_{ij})\, \hat{\mathbf{r}}_{ij} & (r_{ij} < r_c) \\ 0 & (r_{ij} \geq r_c) \end{cases} \tag{2}$$

where a_{ij} is the repulsion energy between beads i and j, r_{ij} is the interbead distance and $\hat{\mathbf{r}}_{ij}$ is the corresponding unit vector. r_c is the cutoff radius. In our DPD and MMC simulations, the particle mass, the temperature and interaction range were chosen as units of mass, energy and length. The weight function $\omega_C(r_{ij})$ is defined to $1 - r_{ij}/r_c$ for $r_{ij} \leq r_c$ and vanishes for $r_{ij} \geq r_c$. The expressions of the different forces can be found in Refs 30,51. The LL interface of the AB system was simulated by placing an equal number particles of A and B in the simulation box. The L_z dimension was fixed to 60 in reduced DPD units corresponding to a reduced number density of 3.0. L_x and L_y were changed from 2.5 to 20.0 in reduced DPD units leading to a variation of a number of particles from 1122 to 72000. The

repulsion a_{AA}, a_{BB} and a_{AB} parameters were fixed to 78.0, 78.0 and 105.0, respectively. The equilibration phase was composed of 10^6 steps and the averages were performed over 5×10^6 steps during the production phase. The thermodynamic properties were calculated every 5 steps leading to the calculation of profiles of pressure components and surface tension over 10^6 configurations. The z-dimension corresponds the dimension normal to the interface.

2.2.2 Generic MMC model

To model a LV interface, the conservative repulsive potential $\omega_C(r_{ij})$ must be modified in order to consider the local density. In the MDPD approach, the conservative force[15,16,50,51] becomes dependent on the local particle density as

$$\mathbf{f}_{ij}^C = A\omega_C(r_{ij})\mathbf{e}_{ij} + B\left[\bar{\rho}_i + \bar{\rho}_j\right]\omega_d(r_{ij})\mathbf{e}_{ij} \tag{3}$$

where the first term represents an attractive interaction ($A < 0$) and the second many-body term a repulsive interaction ($B > 0$). The expressions of the weight functions, the values of the A and B parameters, the values of r_c and r_d are given in Ref. 16. Multibody Monte Carlo (MMC) simulations were carried out using the potential defined by Eq.(4). U^C was calculated from the integration of Eq.(3) where u_i is the energy of particle i and A corresponds to a_{ij} in Eq.(2).

$$\begin{aligned} U^C = \sum_i^N u_i^C = \sum_i^N \Bigg(& \frac{\pi r_c^3}{30} A \sum_{j\neq i} \omega_\rho(r_{ij}, r_c) \\ & + \frac{\pi r_d^4}{30}\left[\sum_{j\neq i} b_{ij}\omega_\rho(r_{ij}, r_d)\left(\omega_\rho(r_{ij}, r_d) + \rho_i^{'} + \rho_j^{'}\right)\right]^2\Bigg) \end{aligned} \tag{4}$$

In Eq.(4) $\rho_i^{'}$ and $\rho_j^{'}$ are defined as

$$\rho_i^{'} = \sum_{k\neq i, k\neq j} \left[1 - \frac{r_{ik}}{r_d}\right]^2, \ \rho_j^{'} = \sum_{k\neq j, k\neq i} \left[1 - \frac{r_{jk}}{r_d}\right]^2 \tag{5}$$

If we assume that $b_{ij} = B$ we obtain the simplified relation

$$U^C = \sum_i^N u_i^C = \sum_i^N \left(\frac{\pi r_c^3}{30} A \sum_{j\neq i} \omega_\rho(r_{ij}, R = r_c) + \frac{\pi r_d^4}{30} B \left[\sum_{j\neq i} \omega_\rho(r_{ij}, R = r_d) \right]^2 \right) \tag{6}$$

The systems were equilibrated during 25×10^6 steps and the average thermodynamic properties were averaged over 25×10^6 additional steps in the constant-NVT ensemble. The simulation boxes were orthorhombic boxes of dimensions $L_x L_y L_z$. The interfacial area is defined by $A = L_x L_y$ where $L_x = L_y$. The MMC simulations used a simulation cell constituted by a number of molecules changing from 1000 to 30000 water beads. In this CG model, a bead corresponds to 4 water molecules. This choice implies that the reduced DPD unit of r_c corresponds to 8.52 Å. The L_x and L_y dimensions were changed from 36 Å to 111 Å. The values of the interaction parameters $a_{ij} = A$ and $b_{ij} = B$ are -50 and 25, respectively. These values have been developed in order to reproduce the surface tension[16] and the coexisting liquid density of water at 298 K.

2.2.3 Realistic DPD model

For the LV interface of the *n*-pentane, the pentane is described by one bead. In this methodology, the potential $\omega_C(r_{ij})$ was replaced by a tabulated potential which has been developed by using a new bayesian strategy.[52,56] The shape of this potential is given for completeness later in the paper in Figure 6a. This CG potential has been used in constant-NVT Monte Carlo simulations with a cutoff radius of 20 Å at two temperatures 300 K and 400 K. 5

$\times 10^5$ cycles of equilibration were performed to stabilize the interface and additional 2×10^6 cycles were carried out to average the coexisting densities and surface tensions. When L_x was changed from 40 Å to 100 Å the total number of beads increased from 1665 to 104411 and L_z was fixed to 500 Å. To study the impact of the change in L_z between 150 and 400 Å, L_x and L_y were fixed to 60 Å.

3 Results and discussions

As discussed in the introduction of this paper, the truncated Lennard-Jones (LJ) potential is associated with a strong dependence of the surface tension on the surface area.[57] Depending on the value of the surface area, the surface tension can vary by ± 20% compared to the value of surface tension (γ_∞) which is defined as the surface tension calculated with the largest surface area (see Figure 1). It means that along this curve, we can observe significant deviations up to 40% between consecutive values of surface tensions. In the case of LJ fluids, it is possible to avoid the size-effects dependence[17] of the surface tension by choosing a surface area of $11 \times 11\sigma^2$. We propose now to investigate the surface area dependence of the surface tension of the MARTINI model for different LV and LL interfaces.

Figure 2a shows the evolution of the surface tension of the LV interface of the *n*-octane at 300 K. The surface tension is calculated from the integral of the profile along the direction normal to the interface of the difference between the normal and tangential components of the pressure tensor.[58–60] For this system, only the repulsion-dispersion interactions are modeled by the use of LJ potential. After a small oscillation with an amplitude of 3 mN m^{-1} that represents a variation of about 15% of the value obtained at the largest interfacial area, the surface tension stabilizes around 19.5 mN m^{-1}. Any size-effects are detected from a surface area of 35×35 Å^2. The comparison with the corresponding LJ truncated potential shows that the surface tension becomes independent of the interfacial area at smaller values for the MARTINI model ($8.5 \times 8.5\sigma^2$ where $\sigma = 4.7$ Å). When electrostatic interactions are

included for the modeling of the LV of water for example (see Figure2b), we observe that the surface tension is subject to small oscillations of 2 mN m^{-1}. The last oscillation is much less marked and extends over 40 Å. The largest interfacial area simulated here is 100×100 Å ($21 \times 21\sigma^2$). If we expect a calculation of the surface tension with an uncertainty of 6%, we can accept an interfacial area of 60×60 $Å^2$. To complete the study with the CG MARTINI force field, we represent in Figure 2c the area dependence of the surface tension in the case of the LL interface of octane-water. The amplitude of the oscillations is again around 2 mN m^{-1} which is in the order of magnitude of the statistical fluctuations. This represents a change in γ of 5% compared to γ_∞. A good convergence of the surface tension with the interfacial area is obtained from a surface of 70×70 $Å^2$. For these three typical interfaces using the CG MARTINI model, we can conclude that the interfacial tension is much less sensitive to size-effects by comparison to the truncated LJ potential. This weak dependence of the surface tension calculated with the MARTINI model can be explained by the fact that this force field uses a truncated and shifted potential avoiding any discontinuity at the cutoff radius. We have already underlined this point in Ref. 35 where the LJ truncated potential, modified by a spline polynomial, removes the discontinuity in the force and energy equations and reduces significantly the anisotropy of the pressure components.

We now investigate the interfacial tension of an oil-water system where the interactions are calculated using a conservative CG model $\frac{1}{2}(1 - r/r_c)^2$ potential which is continuous at the cutoff radius r_c. The simulations were performed using the DPD method. Figure 3a shows the interfacial tension as a function of the interfacial area in reduced DPD units. For a surface area smaller than 5×5, the surface tension shows small oscillations of around 2% and the convergence is obtained from $L_x^* = 10$. Figure 3b shows the profiles of the normal and tangential components of the pressure tensor for two interfacial areas. These profiles represent the total pressure components which sum the kinetic and configurational contributions. As expected from the mechanical equilibrium, the normal and tangential components are equal in the two bulk phases with a negative peak of the tangential part in

the interfacial region. Part c) of Figure 3 displays the profiles of the differences between the normal and tangential components of the pressure tensor at different areas. On the right axis of Figure 3, the integral of these differences are also shown for completeness. The profiles show the same features independently of the surface area : $p_N^*(z^*) - p_T^*(z^*)$ is zero in the bulk liquid phases and present two symmetric peaks at the interfaces. The analysis of $\gamma^*(z^*)$ confirms that the two-phase configurations respect the mechanical equilibrium expected for a planar LL interface. Figure 3c also establishes that the differences in the value of the surface tension cannot be attributed to a lack of convergence of the simulations. By focusing on a specific interface, Figure 3d shows that the profile of $p_N^*(z^*) - p_T^*(z^*)$ is subject to small oscillations at the interface for small interfacial areas. The amplitude of these oscillations decreases with increasing surface areas. For larger surface areas, the profiles do not show any oscillations in the interfacial region whereas their shapes in the bulk phases are much more defined leading to a decrease of the anisotropy of the pressure components.

Figure 4 shows the surface tension of water calculated with a density-dependent CG potential at different surface areas. The parameters of this potential have been optimized through a top-down a procedure to reproduce the surface tension of water calculated by using atomistic models.[16] Simple relationships have been established to link the atomistic and mesoscopic length and time scales and operational parameters have been obtained with the MDPD method to reproduce the surface tension, coexisting densities of water at different temperatures. The degree of coarse-graining was fixed to 4 indicating that a water bead corresponds to 4 water molecules. We propose in Figure 4 to investigate the dependence of the surface tension of water on interfacial areas changing from 40 Å to 120 Å. To make a link with reduced units,[16] the reduced L_x^* should be divided by the cutoff $r_c = 8.52$ Å indicating that L_x^* changes from 4.7 to 14. This curve shows an oscillatory behavior but with a very weak dependence of γ on L_x. No plateau is clearly identifiable on this curve. The maximum and minimum values of γ are 73 and 67 mN m^{-1}, respectively. These deviations correspond to variations of $\pm$ 4% compared to the value of 70 mN m^{-1} over a large range of L_x of 80 Å. The

observed variations are within the statistical fluctuations of the calculation. Let us return to the use of the standard DPD method. We replace the usual conservative potential by a realistic potential model developed from atomistic simulations. The procedure is thoroughly described in Ref. 56 and its application for the calculation of the surface tension of pentane in Ref. 52. In a first step, we study the effects of L_x on the surface tension of the n-pentane at two temperatures. Figure 5a shows that γ decreases slightly with L_x. Actually, γ decreases from 14.4 to 14.1 mN m^{-1} with small oscillations leading to a variation of 3% along the range of L_x values. As shown in Figure 5b for $T = 400K$, we observe a monotonic decrease of γ of 0.45 mN m^{-1} from 40 to 70 Å. For larger interfacial areas, we observe a plateau extending over 30 Å indicating that the surface tension becomes independent of the interfacial area. The $p_N(z) - p_T(z)$, shown in Figure 5c profiles confirms that the mechanical equilibrium of the planar LV is verified for the two interfacial areas. Interestingly, for the smallest L_x value of 40 Å, we observe the profile which is much noisier in the bulk phase leads to a larger surface tension. However, this difference in the surface tension does not come from the contribution of the bulk phase but rather to the interface region on the liquid side as shown in the profile of $\gamma(z)$. The dependence of the surface tension on the longitudinal dimension L_z is shown in Figure 5d. The dependence of γ on L_z is clearly weak from 125 Å to 225 Å with an increase of only 0.2 mN m^{-1}. From $L_z = 250$ Å, we do not observe any monotonic increase of γ. The main conclusions we can draw with the different DPD methods, is that they lead to relatively small dependencies of the surface tension on box dimensions. The differences observed between the different values are on the order of magnitude of the statistical fluctuations.

We plan now to investigate the effect of the truncation on the $\gamma = f(L_x)$ dependence. We do so on using a realistic potential of the pentane developed with a cutoff $r_c = 20$ Å. With $r_c = 20$ Å, the potential decreases smoothly to zero with no discontinuity in the potential as shown in Figure 6a. We take the route of truncating this potential at a smaller value of $r_c = 15$ Å introducing then a discontinuity at this point. We represent in Figure 6b, the

evolution of the ratio of γ to γ_∞ at 400 K where γ_∞ means the surface tension calculated with the largest box dimension L_x. In both cases, the surface tension decreases with L_x but the magnitude of the decrease varies from 30% to 10% as r_c is changing from 20 Å to 15 Å. The introduction of the discontinuity in the potential at 15 Å increases significantly the size-effects on the surface tension. This result is in line with observations made with the LJ potential modified with a cubic spline function.[35]

We complete this study by representing on Figure 7 the ratio γ/γ_∞ for the LV interface of different CG models as a function of the reduced box dimension L_x^*. The reduced value of L_x^* is obtained by dividing the real value by σ for the LJ and MARTINI models, by $r_c = 8.52$ Å for the water MDPD model.[16] For the pentane DPD model, σ is defined by the position of the well of the CG potential represented in Figure 6a. Interestingly, we observe that the LJ potential give rise to large amplitudes of oscillations with a plateau obtained with three successive oscillations. The water MDPD model is also subject to significant oscillations that extend over a wide range of L_x^*. Indeed, these oscillations are not yet stabilized at 22σ even if their amplitude are relatively smaller than those of the LJ fluid. When the MARTINI model is used with only the dispersion-repulsion interactions, *e.g* in the case of the octane molecule, only one oscillation is observed at 6σ. For higher values of the box dimension, there is no more dependence of the surface tension on the surface area. For the mesoscopic simulation methods, the dependence is much less marked. For the water MDPD model, there are small oscillations but we can consider that reduced interfacial areas of 13×13 are acceptable to avoid any size-effects in the calculation of the surface tension. Finally, in the case of the use realistic DPD model, we observe rather a small decrease of the surface tension with the interfacial area. We conclude that a reduced interfacial area of 10×10 is reasonable to avoid any dependence of the surface tension.

4 Conclusions

Since there is a growing demand in the use of CG models for the calculation of the interfacial tension of complex systems and geometries, it was useful to investigate the dependence of the interfacial tension on the surface area for these models. In the case of atomistic models, it is now well-established that the surface tension of Lennard-Jones fluids exhibits an oscillatory behavior as function of the surface area. Relatively large surface area of $11 \times 11\sigma^2$ are required to provide an accurate calculation of the surface tension by using the LJ potential.

We have performed a large number of simulations with different CG models, namely, the MARTINI force field, the standard DPD model and realistic DPD and MDPD models. We have also investigated two types of interfaces : the LV and LL interfaces. Firstly, the size-effects are much less strong with the CG models compared to those observed in atomistic simulations. For the MARTINI model, we observe a weak oscillatory effect with small fluctuations for the LV and LL interfaces. This weak dependence is also observed in the LL interface with the standard DPD model. In the case of the MDPD model for water, the LV surface tension exhibits also a weak oscillatory behavior with small amplitudes. When we use a realistic model for the DPD, we observe that the slight oscillatory behavior observed at 300 K is replaced by a monotonic decrease of γ at T= 400 K. We show here that the truncation impacts the dependence of the surface tension on the surface area as already underlined for atomistic models.

At the end, we give some recommendations to avoid any size-effects of these models by plotting the surface tension as a function of the reduced interfacial area. The differences that appear on the interfacial area dependence with the MARTINI model find their origin in the use of the electrostatic interactions. The surface tension is much less dependent on the surface area with the DPD model even if the water MDPD model is much sensitive to size-effects.

References

(1) Arnarez, C.; Uusitalo, J. J.; Masman, M. F.; Ingolfsson, H. I.; de Jong, D. H.; Melo, M. N.; Periole, X.; de Vries, A. H.; Marrink, S. J. Dry Martini, a Coarse-Grained Force Field for Lipid Membrane Simulations with Implicit Solvent. *J. Chem. Theory. Comput*. **2014**, *11*, 260–275.

(2) Maurel, G.; Goujon, F.; Schnell, B.; Malfreyt, P. Prediction of Structural and Thermomechanical Properties of Polymers from Multiscale Simulations. *RSC Adv*. **2015**, *5*, 14065–14073.

(3) Maurel, G.; Goujon, F.; Schnell, B.; Malfreyt, P. Multiscale Modeling of the Polymer-Silica Surface Interaction: from Atomistic to Mesoscopic Simulations. *J. Phys. Chem. C* **2015**, *119*, 4817–4826.

(4) Espanol, P.; Warren, P. Perspective: Dissipative Particle Dynamics. *J. Chem. Phys*. **2017**, *146*, 150901.

(5) Ndao, M.; Goujon, F.; Ghoufi, A.; Malfreyt, P. Coarse–Grained Modeling of the Oil–Water–Surfactant Interface Through the Local Definition of the Pressure Tensor and Interfacial Tension. *Theor. Chem. Acc*. **2017**, *136*, 21.

(6) Marrink, S. J.; de Vries, A. H.; Mark, A. E. Coarse Grained Model for Semiquantitative Lipid Simulations. *J. Phys. Chem. B* **2004**, *108*, 750–760.

(7) Marrink, S. J.; Risselada, H. J.; Yefimov, S.; Tieleman, D. P.; de Vries, A. H. The MARTINI Force Field: Coarse Grained Model for Biomolecular Simulations. *J. Phys. Chem. B* **2007**, *111*, 7812–7824.

(8) Monticelli, L.; Kandasamy, S. K.; Periole, X.; Larson, R. G.; Tieleman, D. P.; Marrink, S. J. The MARTINI Coarse-Grained Force Field: Extension to Proteins. *J. Chem. Theory Comput*. **2008**, *4*, 819–834.

(9) Lopez, C. A.; Rzepiela, A. J.; de Vries, A. H.; Dijkhuizen, L.; Hünenberger, P. H.; Marrink, S. J. Martini Coarse-Grained Force Field: Extension to Carbohydrates. *J. Chem. Theory Comput.* **2009**, *5*, 3195–3210.

(10) Yesylevskyy, S. O.; Schäfer, L. V.; Sengupta, D.; Marrink, S. J. Polarizable Water Model for the Coarse-Grained MARTINI Force Field. *PLoS Comp. Biol.* **2010**, *6*, 1–17.

(11) Sergi, D.; Scocchi, G.; Ortona, A. Coarse-Graining MARTINI Model for Molecular-Dynamics Simulations of the Wetting Properties of Graphitic Surfaces with Non-Ionic, Long-Chain, and T-Shaped Surfactants. *J. Chem. Phys.* **2012**, *137*, 094904.

(12) Marrink, S. J.; Tieleman, D. P. Perspective on the Martini Model. *Chem. Soc. Rev.* **2013**, *42*, 6801–6822.

(13) Hoogerbrugge, P. J.; Koelman, J. M. V. A. Simulating Microscopic Hydrodynamic Phenomena with Dissipative Particle Dynamics. *Europhys. Lett.* **1992**, *19*, 155–160.

(14) Groot, R. D.; Warren, P. B. Dissipative Particle Dynamics: Bridging the Gap Between Atomistic and Mesoscopic Simulation. *J. Chem. Phys.* **1997**, *107*, 4423–4435.

(15) Warren, P. B. Vapor-Liquid Coexistence in Many-Body Dissipative Particle Dynamics. *Phys. Rev. E* **2003**, *68*, 066702.

(16) Ghoufi, A.; Malfreyt, P. Mesoscale Modeling of the Water Liquid–Vapor Interface: A Surface Tension Calculation. *Phys. Rev. E* **2011**, *83*, 051601.

(17) Ghoufi, A.; Malfreyt, P.; Tildesley, D. J. Computer Modelling of the Surface Tension of the Gas-Liquid and Liquid-Liquid Interface. *Chem. Soc. Rev.* **2016**, *45*, 1387–1409.

(18) Ndao, M.; Devemy, J.; Ghoufi, A.; Malfreyt, P. Coarse-Graining the Liquid-Liquid Interfaces with the MARTINI Force Field : How is The Interfacial Tension Reproduced ? *J. Chem. Theory. Comput.* **2015**, *11*, 3818–3828.

(19) Jasper, J. J. The Surface Tension of Pure Liquid Compounds. *J. Phys. Chem. Ref. Data* **1972**, *1*, 841–1009.

(20) Vasquez, G.; Alvarez, E.; Navaza, J. M. Surface Tension of Alcohol + Water from 20 to 50 °C. *J. Chem. Eng. Data* **1995**, *40*, 611–614.

(21) Liu, K. S. Phase Separation of Lennard-Jones Systems: A Film in Equilibrium with Vapor. *J. Chem. Phys.* **1974**, *60*, 4226–4230.

(22) Lee, J. K.; Barker, J. A.; Pound, G. M. Surface Structure and Surface Tension: Perturbation Theory and Monte Carlo Calculation. *J. Chem. Phys.* **1974**, *60*, 1976–1980.

(23) Chapela, G. A.; Saville, G.; Rowlinson, J. Computer-Simulation of Gas-Liquid Surface. *Discuss. Faraday Soc.* **1975**, *59*, 22–28.

(24) Rao, M.; Levesque, D. Surface-Structure of a Liquid-Film. *J. Chem. Phys.* **1976**, *65*, 3233–3236.

(25) Chapela, G. A.; Saville, G.; Thompson, S. M.; Rowlinson, J. S. Computer-Simulation of a Gas-Liquid Surface. 1. *J. Chem. Soc. Faraday Trans. II* **1977**, *73*, 1133–1144.

(26) Salomons, E.; Mareschal, M. Atomistic Simulation of Liquid-Vapour Coexistence:Binary Mixtures. *J. Phys. Condens. Matter* **1991**, *3*, 9215–9228.

(27) Blokhuis, E. M.; Bedaux, D.; Holcomb, C. D.; Zollweg, J. A. Tail Corrections to the Surface Tension of a Lennard-Jones Liquid-Vapour Interface. *Molec. Phys.* **1995**, *85*, 665–669.

(28) Guo, M.; Lu, B. Long Range Corrections to Thermodynamic Properties of Inhomogeneous Systems with Planar Interfaces. *J. Chem. Phys.* **1997**, *106*, 3688–3695.

(29) Goujon, F.; Malfreyt, P.; Boutin, A.; Fuchs, A. H. Direct Monte Carlo Simulations of the Equilibrium Properties of n-Pentane Liquid–Vapor Interface. *J. Chem. Phys.* **2002**, *116*, 8106–8117.

(30) Goujon, F.; Malfreyt, P.; Tildesley, D. J. Dissipative Particle Dynamics Simulations in the Grand Canonical Ensemble: Applications to Polymer Brushes. *ChemPhysChem* **2004**, *5*, 457–464.

(31) Holcomb, C. D.; abd J. A. Zollweg, P. C. A Critical Study of the Simulation of the Liquid-Vapour Interface of a Lennard-Jones Fluid. *Mol. Phys.* **2006**, *78*, 437–459.

(32) Janeček, J.; Krienke, H.; Schmeer, G. Interfacial Properties of Cyclic Hydrocarbons: A Monte Carlo Study. *J. Phys. Chem. B* **2006**, *110*, 6916–6923.

(33) Ibergay, C.; Ghoufi, A.; Goujon, F.; Ungerer, P.; Boutin, A.; Rousseau, B.; Malfreyt, P. Molecular Simulations of the n-Alkane Liquid-Vapor Interface: Interfacial Properties and Their Long Range Corrections. *Phys. Rev. E* **2007**, *75*, 051602.

(34) Shen, V. K.; Mountain, R. D.; Errington, J. R. Comparative Study of the Effect of Tail Corrections on Surface Tension Determined by Molecular Simulation. *J. Phys. Chem. B* **2007**, *111*, 6198–6207.

(35) Biscay, F.; Ghoufi, A.; Goujon, F.; Lachet, V.; Malfreyt, P. Calculation of the Surface Tension from Monte Carlo Simulations: Does the Model Impact on the Finite-Size Effects? *J. Chem. Phys.* **2009**, *130*, 184710.

(36) Ferrando, N.; Lachet, V.; Pérez-Pellitero, J.; Mackie, A. D.; Malfreyt, P.; Boutin, A. A Transferable Force Field to Predict Phase Equilibria and Surface Tension of Ethers and Glycol Ethers. *J. Phys. Chem. B* **2011**, *115*, 10654–10664.

(37) Werth, S.; Lishchuk, S. V.; Horsch, M.; Hasse, H. The Inflence of the Liquid Slab Thickness on the Planar Vapor-Liquid Interfacial Tension. *Physica A* **2013**, *392*, 2359–2367.

(38) Míguez, J. M.; Piñeiro, M. M.; Blas, F. J. Influence of the Long-Range Corrections on

the Interfacial Properties of Molecular Models using Monte Carlo Simulation. *J. Chem. Phys.* **2013**, *138*, 34707–34716.

(39) Trokhymchuk, A.; Alejandre, J. Computer Simulations of Liquid/Vapor Interface in Lennard-Jones Fluids: Some Questions and Answers. *J. Chem. Phys.* **1999**, *111*, 8510–8523.

(40) Lopez-Lemus, J.; Alejandre, J. Thermodynamic and Transport Properties of Simple Fluids using Lattice Sums: Bulk Phases and Liquid-Vapour Interface. *Mol. Phys.* **2002**, *100*, 2983–2992.

(41) Grosfils, P.; Lutsko, J. F. Dependence of the Liquid-Vapor Surface Tension on the Range of Interaction: A Test of the Law of Corresponding States. *J. Chem. Phys.* **2009**, *130*, 054703.

(42) Gloor, G. J.; Jackson, G.; Blas, F. J.; de Miguel, E. Test-Area Simulation Method for the Direct Determination of the Interfacial Tension of Systems with Continuous or Discontinuous Potentials. *J. Chem. Phys.* **2005**, *123*, 134703–134721.

(43) Ghoufi, A.; Malfreyt, P. Entropy and Enthalpy Calculations from Perturbation and Integration Thermodynamics Methods using Molecular Dynamics Simulations: Applications to the Calculation of Hydration and Association Thermodynamic Properties. *Mol. Phys.* **2006**, *104*, 2929–2943.

(44) Ghoufi, A.; Goujon, F.; Lachet, V.; Malfreyt, P. Multiple Histogram Reweighting Method for the Surface Tension Calculation. *J. Chem. Phys.* **2008**, *128*, 154718.

(45) Guo, M.; Peng, B. Y.; Lu, C. Y. On the Long-Range Corrections to Computer Simulation Results for the Lennard-Jones Vapor-Liquid Interface. *Fluid Phase Equilibria* **1997**, *130*, 19–30.

(46) Orea, P.; Lopez-Lemus, J.; Alejandre, J. Oscillatory Surface Tension due to Finite-Size Effects. *J. Chem. Phys.* **2005**, *123*, 114702.

(47) Gonzalez-Melchor, M.; Orea, P.; Lopez-Lemus, J.; Bresme, F.; Alejandre, J. Stress Anisotropy Induced by Periodic Boundary Conditions. *J. Chem. Phys.* **2005**, *122*, 094503.

(48) Velazquez, M. E.; Gama-Goicochea, A.; Conzalez-Melchor, M.; Neria, M.; Alejandre, J. Finite-Size Effects in Dissipative Particle Dynamics Simulations. *J. Chem Phys.* **2006**, *124*, 084104.

(49) Errington, J. R.; Kofke, D. A. Calculation of Surface Tension via Area Sampling. *J. Chem. Phys.* **2007**, *127*, 174709.

(50) Ghoufi, A.; Malfreyt, P. Coarse Grained Simulations of the Electrolytes at the Water/Air Interface from Many Body Dissipative Particle Dynamics. *J. Chem. Theory Comput.* **2012**, *8*, 787–791.

(51) Ghoufi, A.; Malfreyt, P. Recent Advances in Many Body Dissipative Particles Dynamics Simulations of Liquid-Vapor Interfaces. *Eur. Phys. J. E* **2013**, *36*, 10.

(52) Canchaya, J. G. S.; Dequidt, A.; Goujon, F.; Malfreyt, P. Development of DPD Coarse-Grained Models: from Bulk to Interfacial Properties. *J. Chem Phys.* **2016**, *145*, 054107.

(53) Todorov, I.; and, W. S. D_LPOLY_3: New Dimensions in Molecular Dynamics Simulations via Massive Parallelism. *J. Mater. Chem.* **2006**, *16*, 1911–1918.

(54) Nosé, S. A Molecular Dynamics Method for Simulations In the Canonical Ensemble. *Molec. Phys.* **1984**, *52*, 255–268.

(55) Nosé, S.; Klein, M. Constant Pressure Molecular Dynamics for Molecular Systems. *Molec. Phys.* **1983**, *50*, 1055–1076.

(56) Dequidt, A.; Canchaya, J. G. S. Bayesian Parametrization of Coarse-Grain Dissipative Dynamics Models. *J. Chem Phys.* **2015**, *143*, 084122.

(57) d'Oliveira, H. D.; Davoy, X.; Arche, E.; Malfreyt, P.; Ghoufi, A. Test-Area Surface Tension Calculation of the Graphene-Methane Interface: Fluctuations and Commensurability. *J. Chem. Phys* **2017**, *146*, 214112.

(58) Kirkwood, J. G.; Buff, F. P. The Statistical Mechanical Theory of Surface Tension. *J. Chem. Phys.* **1949**, *17*, 338–343.

(59) Irving, J. H.; Kirkwood, J. The Statistical Mechanical Theory of Transport Processes .IV. The Equations of Hydrodynamics. *J. Chem. Phys.* **1950**, *18*, 817–829.

(60) Rowlinson, J. S.; Widom, B. *Molecular Theory of Capillarity*; Clarendon Press: Oxford, 1982.

Table 1: Lennard-Jones parameters and electrostatic charges for different molecules described through the MARTINI force field.

CG bead	AA	σ (nm)	ϵ (kJ mol^{-1})	q (e)
		Water		
W	4 H_20	0.47	4.0	0
WP		0	0	0.46
WM		0	0	-0.46
distance W-WP, W-WM (nm)	0.14			
angle WP-W-WM (rad)	$\theta_0 = 0$	$k_\theta = 4.2$ K mol^{-1} rad^{-2}		
		n-octane		
C1	C-C-C-C	0.47	3.5	0
distance C1-C1 (nm)	$r_0 = 0.47$	$k_b = 1250$ kJ mol^{-1} nm^{-2}		
		Matrix of crossed-interactions		
Site	Site	σ (nm)	ϵ (kJ mol^{-1})	
C1	W	0.47	1.9	

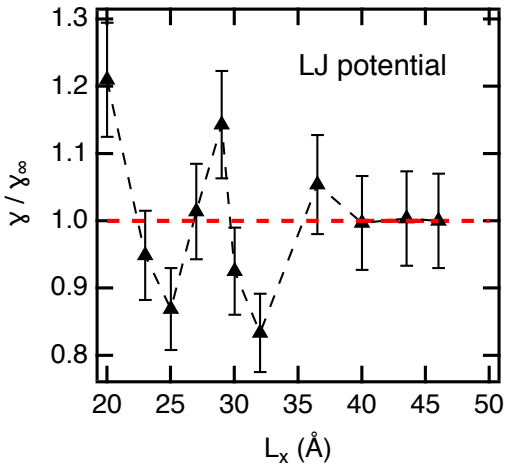

Figure 1: Ratio of the surface tension γ to the value of γ_∞ for different L_x box dimensions. γ_∞ is calculated with the interfacial area $A = L_x L_y = 46 \times 46$ Å^2. The data can be found in Ref. 35 and correspond to the values of methane at T = 120 K. The cutoff was fixed to $r_c = 2.5\sigma$.

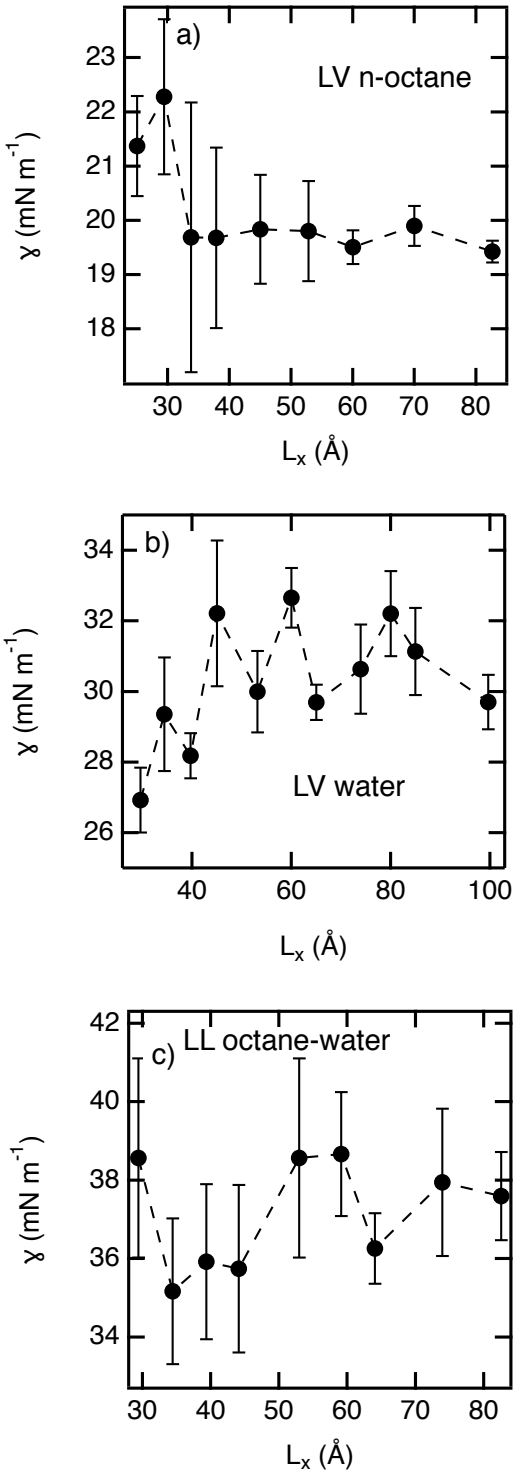

Figure 2: Surface tensions of the LV interfaces of the a) n-octane and b) water. c) Surface tension of the LL interface of the n-octane-water system. The surface tensions are calculated at different box dimensions L_x defined by $\sqrt{A}$ where A is the surface area.

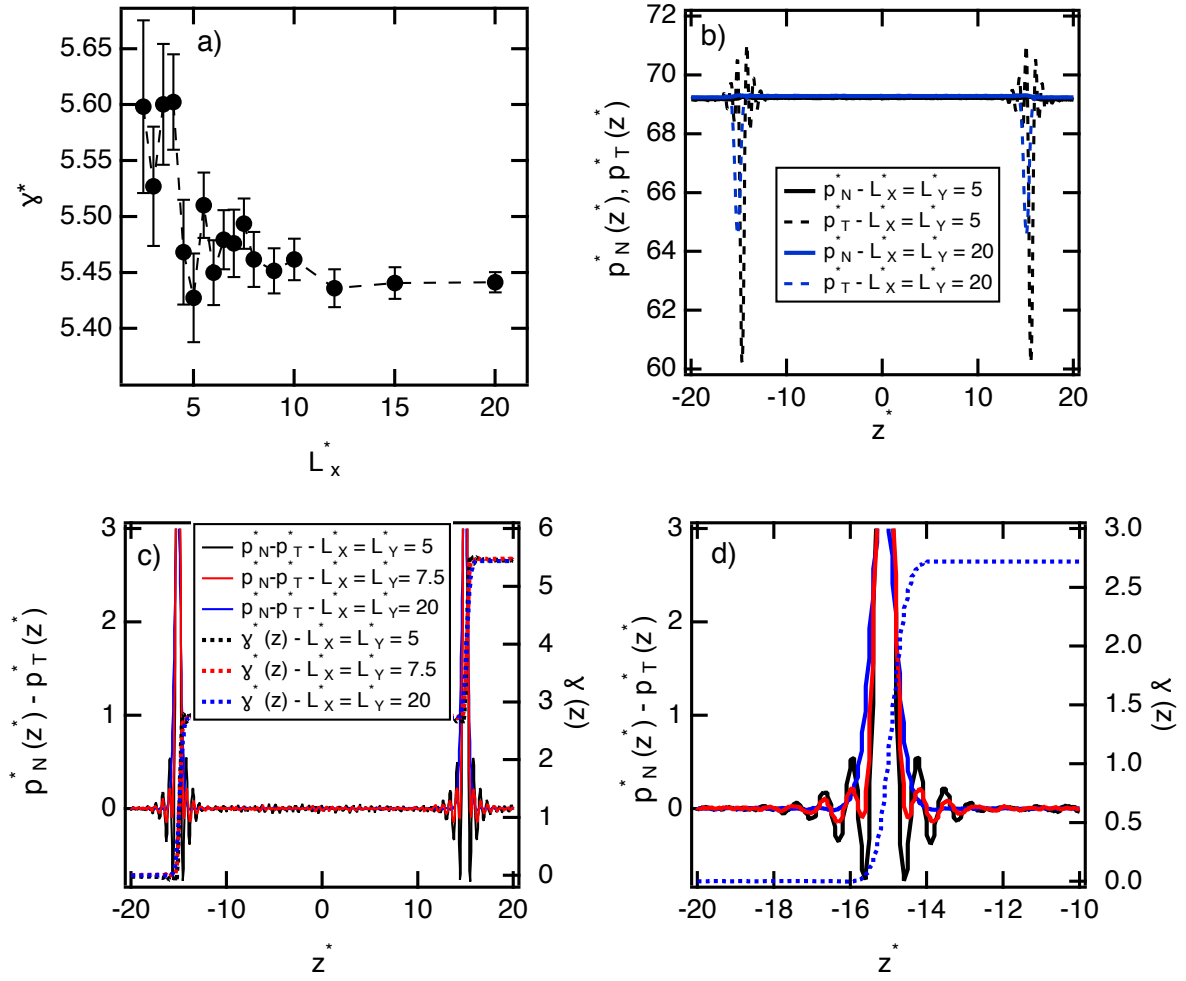

Figure 3: a) Reduced surface tensions of the oil-water LL water calculated using the DPD method as a function of the reduced L^*_x dimension. b) Profiles of the normal $p^*_N(z^*)$ and tangential $p^*_T(z^*)$ reduced pressure components for two interfacial areas. c) Profiles of the difference between the normal and tangential reduced pressure components with the integral $\gamma^*(z^*)$ of this property as a function of z^*. d) Close-up view of the pressure and surface tension profiles at only one interfacial region. All the units are given in reduced DPD units.

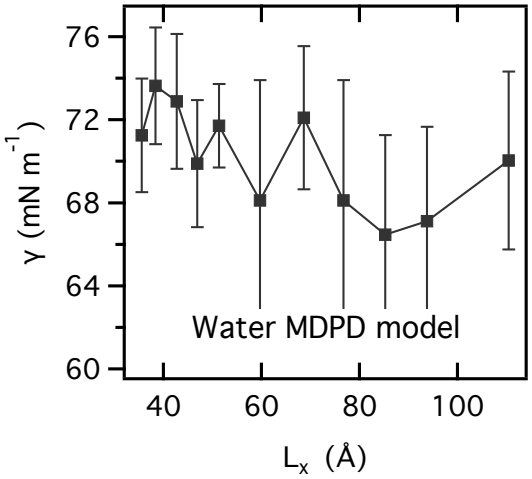

Figure 4: Values of surface tension (mN m^{-1}) of water calculated with MDPD simulation as a function of the box dimension along the x-dimension.

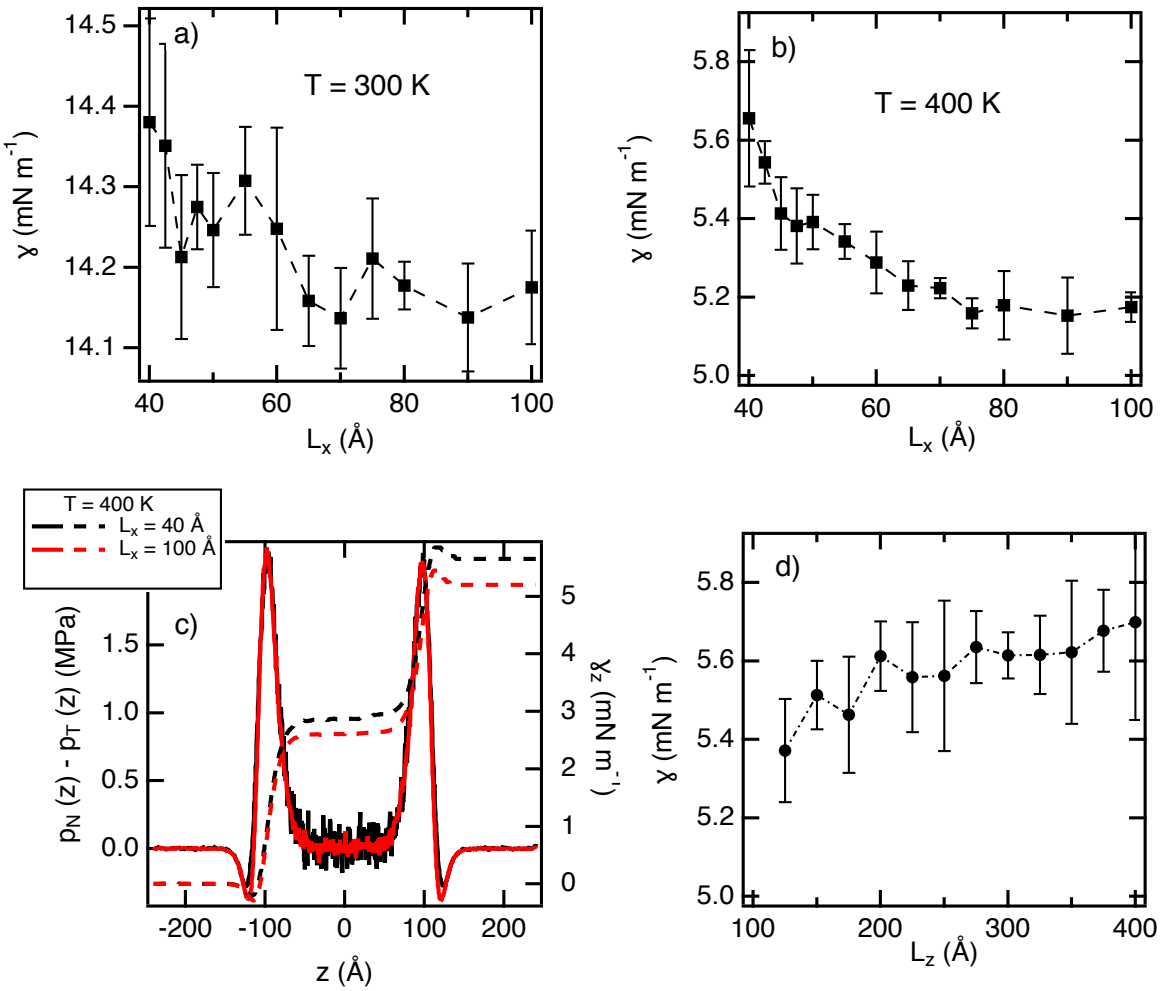

Figure 5: Surface tensions of the n-pentane calculated using a realistic tabulated DPD potential at a) 300 K and b) 400 K. c) Profiles of the difference $p_N(z) - p_T(z)$ at T= 400 K for two box dimensions. d) Surface tensions calculated at different longitudinal dimensions L_z at 400 K.

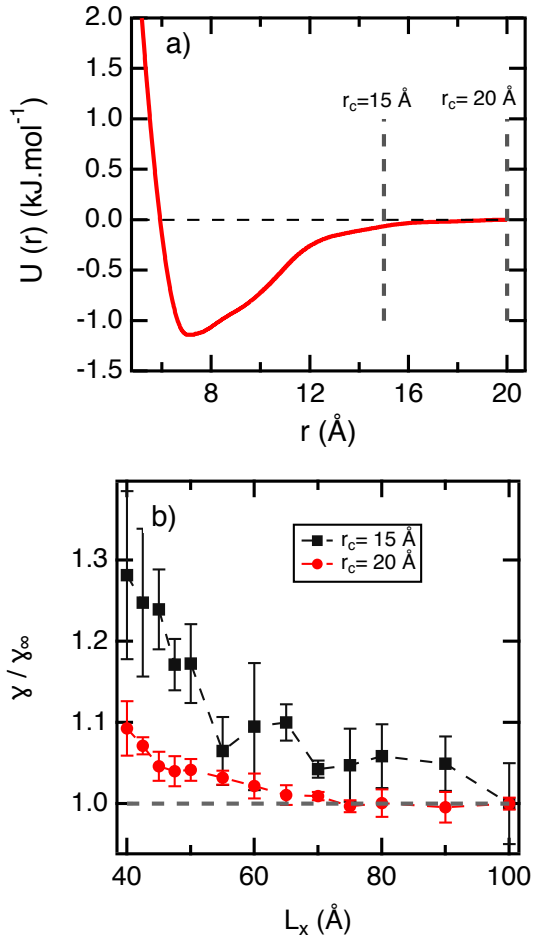

Figure 6: a) Coarse-grained realistic tabulated potential between pentane molecules as a function of the distance. The cutoff radius is indicated for clarity. b) Ratio of the surface tension γ to the value of γ_∞ calculated for the CG potential truncated at $r_c = 15$ Å and $r_c = 20$ Å at 400 K.

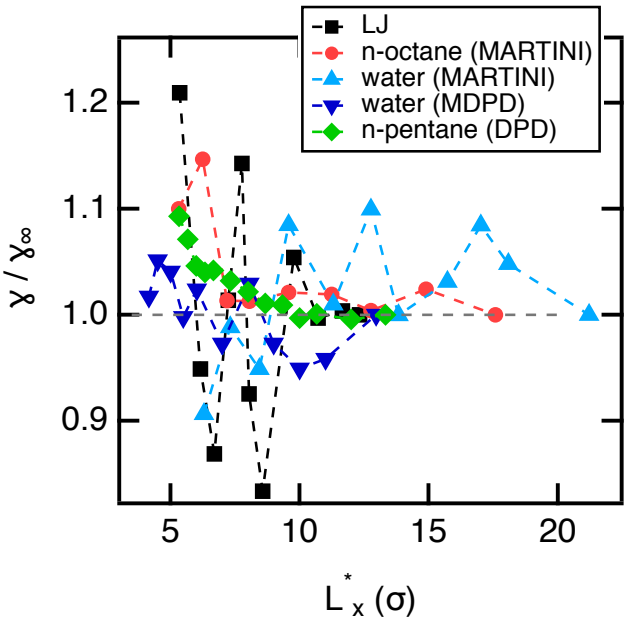

Figure 7: Ratio of the surface tension γ to the value γ_∞ calculated at the largest L_x box dimensions for the LV interfaces of different systems and models as indicated in the legend. The horizontal axis is represented in reduced units of L_x. For the LJ and MARTINI models, the reduced L_x^* is equal to L_x/σ. For the water MDPD model, the reduced box dimension is L_x/r_c where r_c is 8.52 Å (see Ref. 16). For the n-pentane DPD model, L_x is divided by σ where σ represents the position of the well of the potential (see Figure 6a).

Graphical TOC Entry

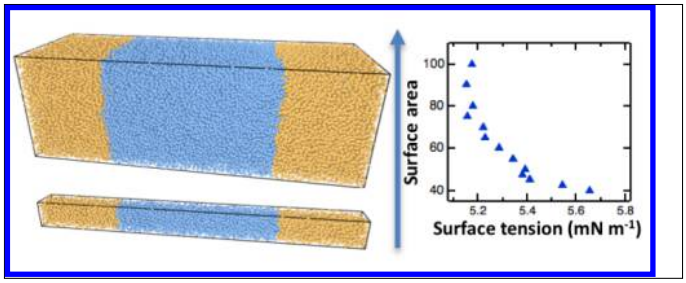

Table of Contents use only
How does the surface tension depend on the surface area with coarse-grained models ?
Florent Goujon, Alain Dequidt, Aziz Ghoufi, Patrice Malfreyt

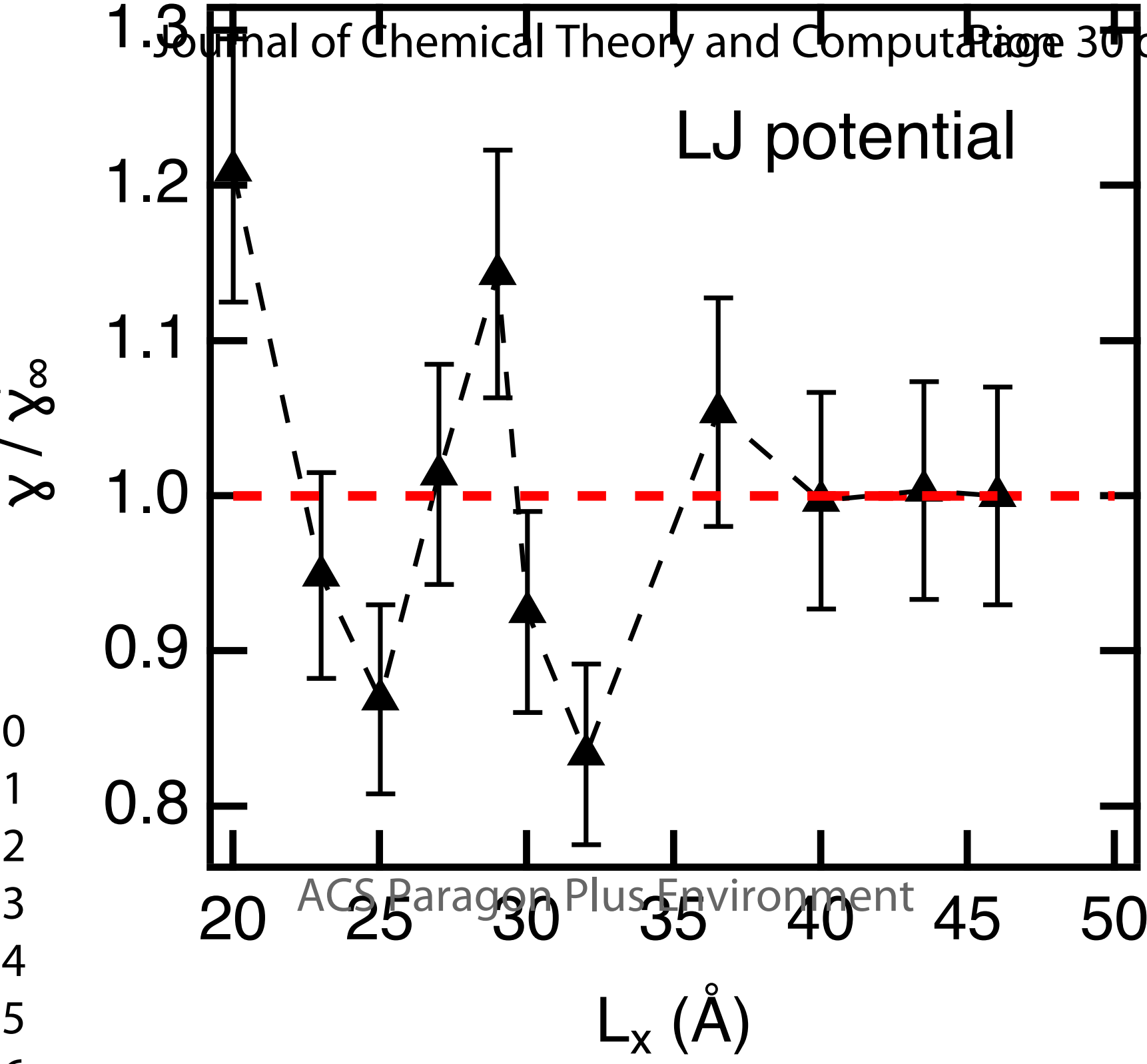

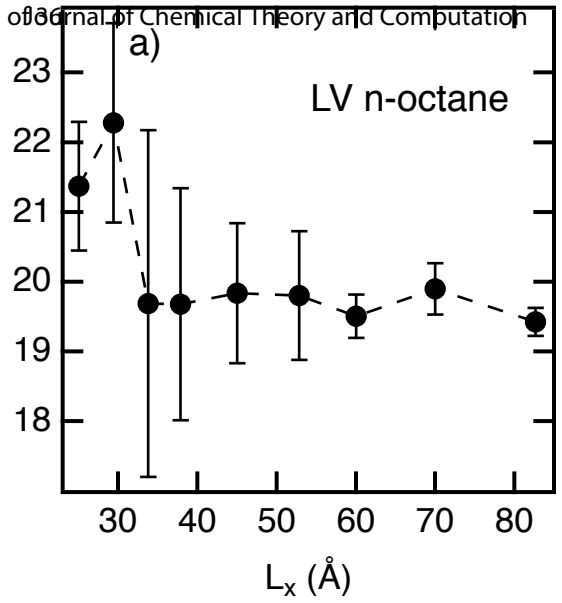

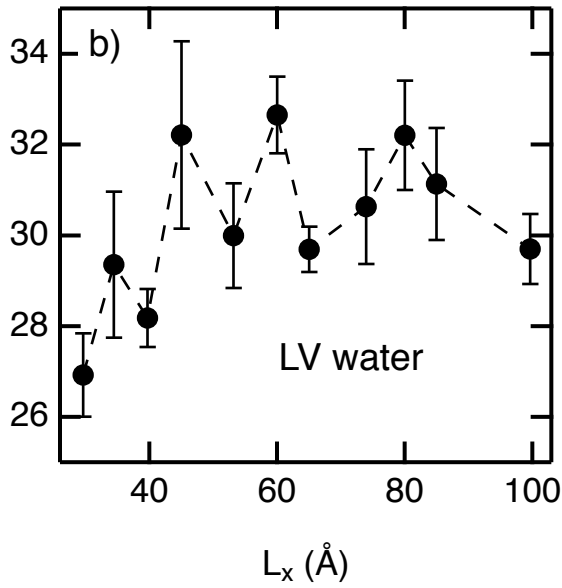

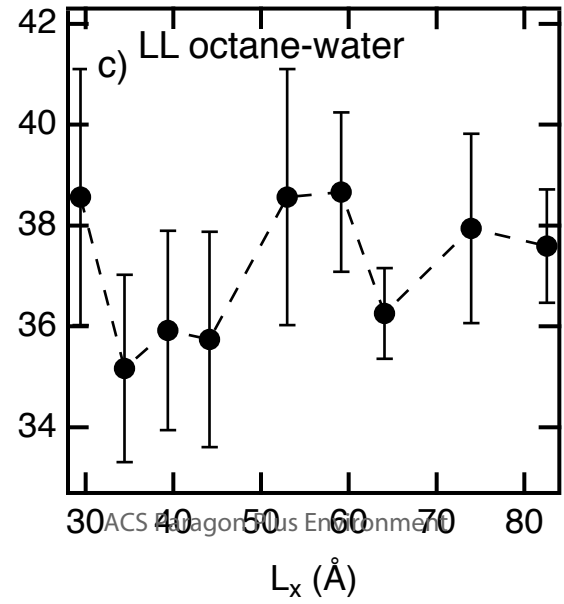

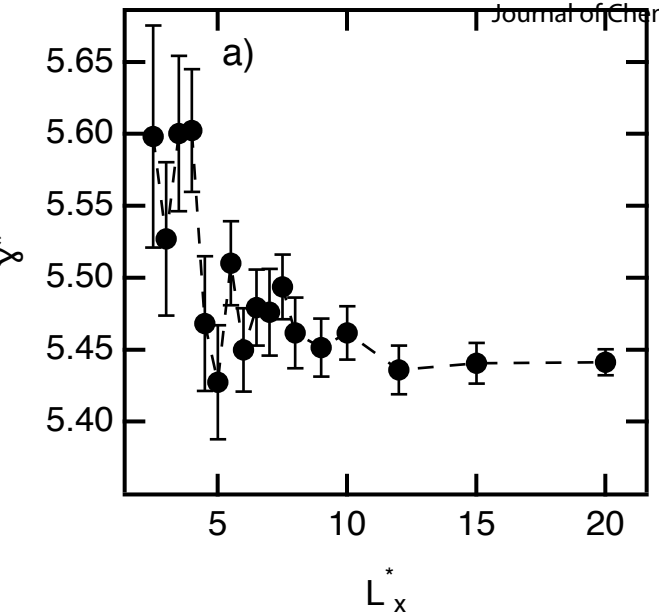
a)
5.65
5.60
5.55
5.50
5.45
5.40
γ*
5
10
15
20
L*x

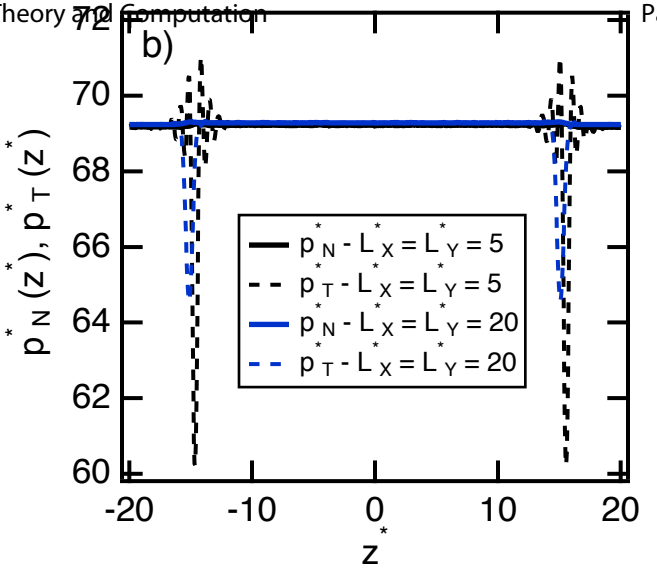
b)
72
70
68
66
64
62
60
p*N(z*), p*T(z*)
-20
-10
0
10
20
z*
p*N - L*X = L*Y = 5
p*T - L*X = L*Y = 5
p*N - L*X = L*Y = 20
p*T - L*X = L*Y = 20

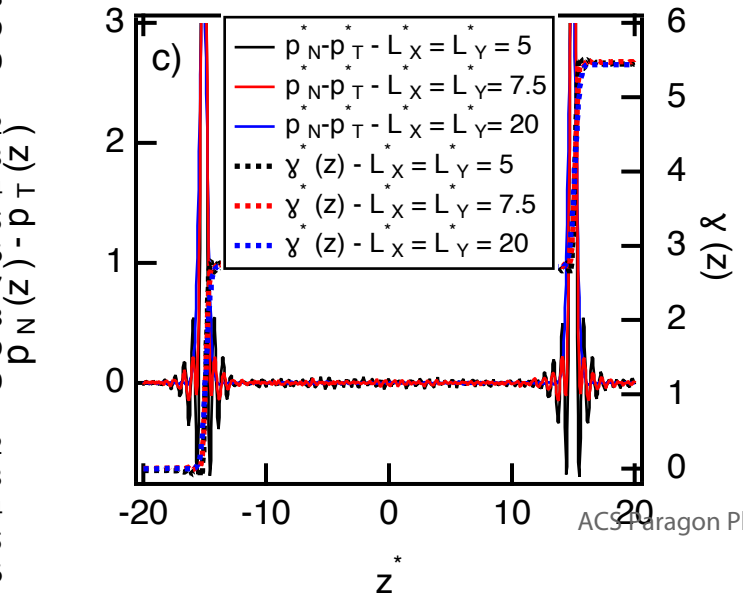
c)
3
2
1
0
p*N(z*) - p*T(z*)
6
5
4
3
2
1
0
γ (z)
-20
-10
0
10
20
z*
p*N-p*T - L*X = L*Y = 5
p*N-p*T - L*X = L*Y= 7.5
p*N-p*T - L*X = L*Y= 20
γ*(z) - L*X = L*Y = 5
γ*(z) - L*X = L*Y = 7.5
γ*(z) - L*X = L*Y = 20

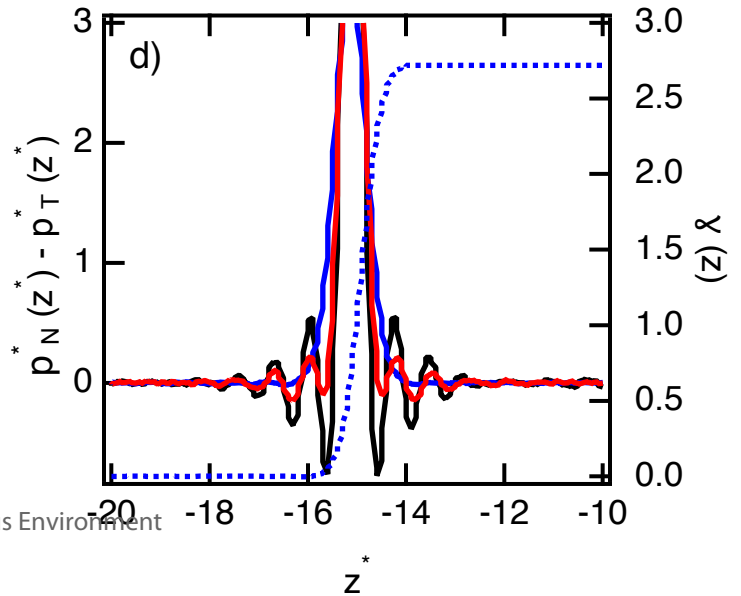
d)
3
2
1
0
p*N(z*) - p*T(z*)
3.0
2.5
2.0
1.5
1.0
0.5
0.0
γ (z)
-20
-18
-16
-14
-12
-10
z*

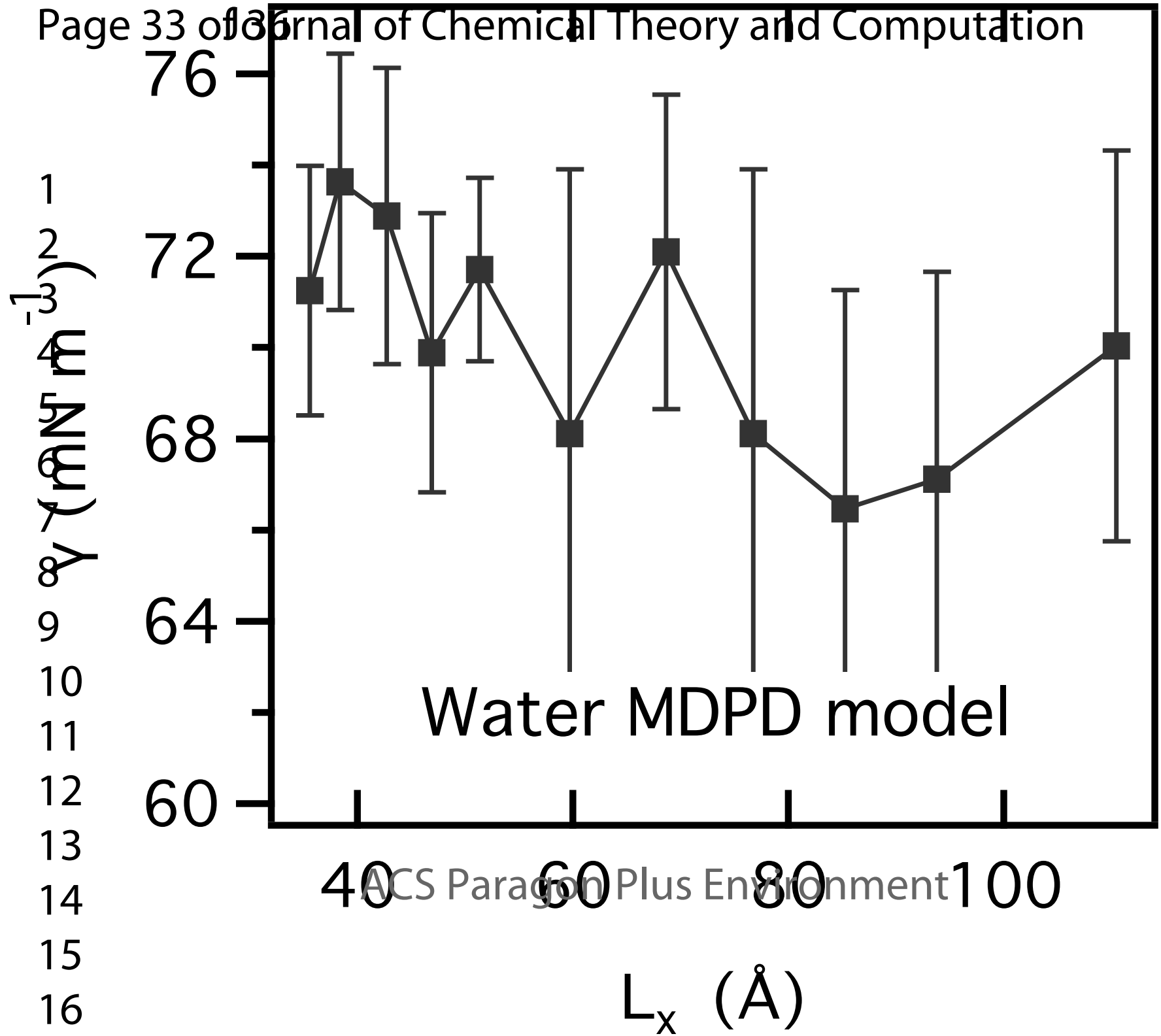

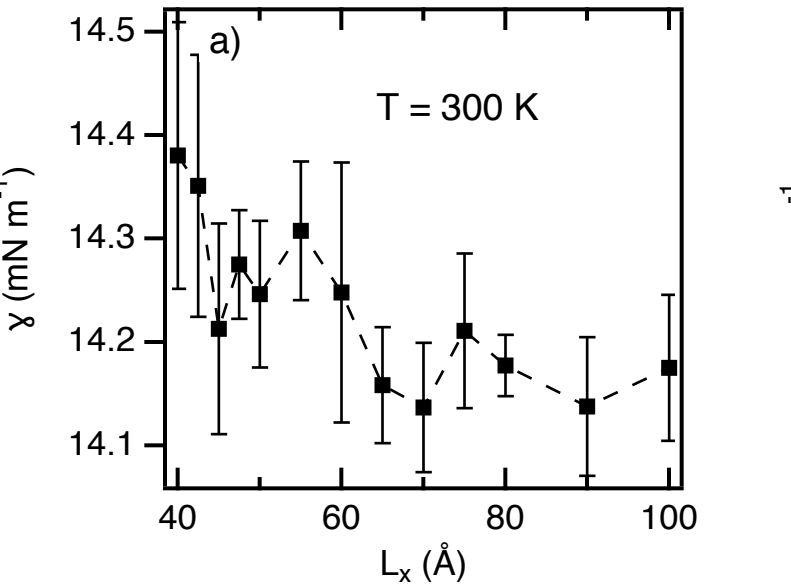
a)
T = 300 K
γ (mN m-1)
Lx (Å)

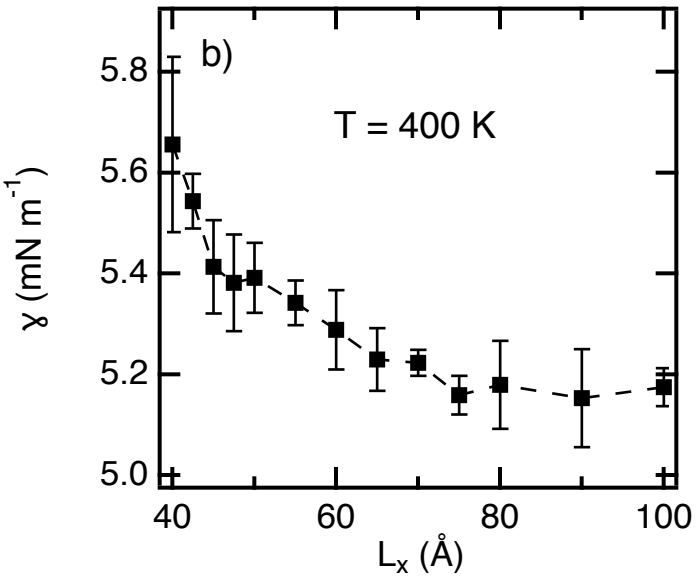
b)
T = 400 K
γ (mN m-1)
Lx (Å)

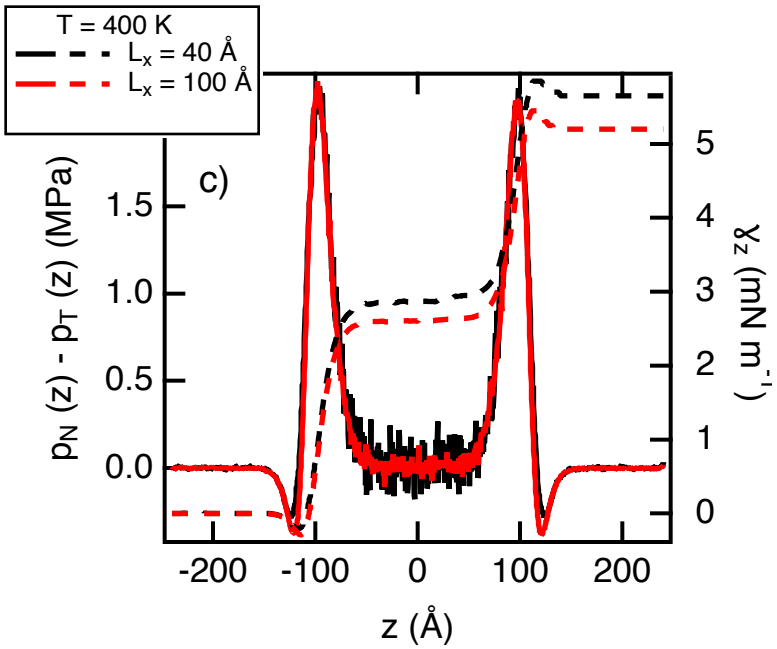
T = 400 K
Lx = 40 Å
Lx = 100 Å
c)
pN (z) - pT (z) (MPa)
χz (mN m-1)
z (Å)

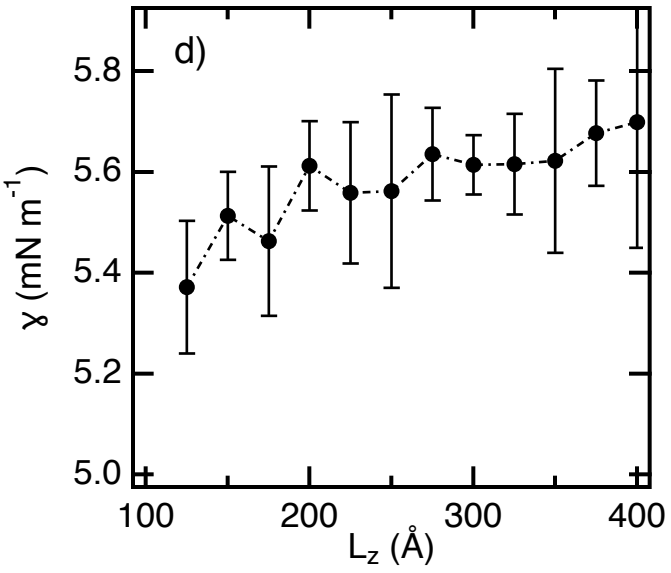
d)
γ (mN m-1)
Lz (Å)